Ultrastable Carboxyl-Functionalized Pore-Space-Partitioned Metal-Organic Frameworks for Gas Separation

Pooja Ajayan,[a] Dr. Wei Wang,[a] Yichong Chen,[a] Prof. Xianhui Bu,[b] and Prof. Pingyun Feng *[a]*

Pooja Ajayan, Dr. Wei Wang, Yichong Chen, Prof. Pingyun Feng
Department of Chemistry, University of California, Riverside, California 92521, United States
E-mail: pingyun.feng@ucr.edu
Prof. Xianhui Bu
Department of Chemistry and Biochemistry, California State University, Long Beach, California 90840, United States
E-mail: xianhui.bu@csulb.edu

Keywords: multi-module MOF, pore space partition, carboxyl functionalization, ultrastability, gas separation

Isoreticular chemistry, which enables property optimization by changing compositions without changing topology, is a powerful synthetic strategy. One of the biggest challenges facing isoreticular chemistry is to extend it to ligands with strongly coordinating substituent groups such as unbound -COOH, because competitive interactions between such groups and metal ions can derail isoreticular chemistry. It is even more challenging to have an isoreticular series of carboxyl-functionalized MOFs capable of encompassing chemically disparate metal ions. Here, with simultaneous introduction of carboxyl functionalization and pore space partition, we have developed a family of carboxyl-functionalized materials in diverse compositions from homometallic Cr^{3+} and Ni^{2+} to heterometallic Co^{2+}/V^{3+}, Ni^{2+}/V^{3+}, Co^{2+}/In^{3+}, Co^{2+}/Ni^{2+}. Cr-MOFs remain highly crystalline in boiling water. Unprecedentedly, one Cr-MOF can withstand the treatment cycle with 10 M NaOH and 12 M HCl, allowing reversible inter-conversion between unbound -COOH acid form and $-COO^-$ base form. These materials exhibit excellent sorption properties such as high uptake capacity for CO_2 (100.2 cm^3/g) and hydrocarbon gases

(e.g., 142.1 cm^3/g for C_2H_2, 110.5 cm^3/g for C_2H_4) at 1 bar and 298K, high benzene/cyclohexane selectivity (up to about 40), and promising separation performance for gas mixtures such as C_2H_2/CO_2 and C_2H_2/C_2H_4.

1. Introduction

The concept of isoreticular chemistry is among the most useful design strategies for metal-organic frameworks. [1–4] Isoreticular MOF chemistry is usually understood as changing framework building blocks while retaining topological types. [5,6] A common practice in isoreticular chemistry is to use ligands of different lengths or with different substituent groups. Changing metal ions is another method.[7,8] Isoreticular chemistry has been shown to be effective to tune pore size, pore shape, pore volume, and pore functionality, leading to dramatically improved properties such as gas uptake capacity, gas selectivity, and chemical stability.[7,9–11] However, there are varying degrees of limitations when deploying isoreticular strategy on different MOF platforms. Past research has shown that different MOF platforms exhibit different levels of tolerance towards attempted isoreticular replacement.[12–14] Noticeably, few MOF platforms are capable of isoreticular chemistry under some challenging situations. One such challenging situation is the creation of isoreticular MOF series that contain unbound functional groups (e.g., -COOH). Such functional groups possess strong coordination capability comparable to or even exceed (e.g., when the chelating mode becomes possible due to such unbound groups being adjacent to the bound groups) those used for the framework formation. In rare cases when such unbound groups do get included, it is another level of difficulty to expand metal ion types to include diverse metal compositions from homometallic M^{3+} to M^{2+} to heterometallic M^{2+}/M^{3+} combinations.[15–17] This difficulty in expanding isoreticular series lies in the myriad of possible coordination modes between polyfunctional ligands and various metal ions, which create multiple unintended crystallization pathways and makes it difficult to direct the crystallization process towards the targeted isoreticular series.

One way to address the aforementioned challenge in isoreticular expansion is to develop an isoreticular platform with various embedded structure-directing effects among framework components, for example, by developing multi-module MOF platforms. The synergy between different modules can create strong inter-modular structure-directing effects that can make the overall assembly more accommodative to the change in each individual module. This strategy requires us to think beyond the traditional two-module platforms (one type of inorganic node

and one type of organic node) to which most well-known MOF structures belong (e.g., monomeric-M ZIF-8,[18] dimeric-M_2 HKUST-1,[19] trimeric-M_3 MIL-88/100/101[20,21] and soc-MOFs,[22] tetrameric-M_4 MOF-5,[23] hexameric-M_6 UiO-66,[24] chain-type MIL-53/MIL-160/MOF-74).[25–27] However, multi-module MOF platforms also exhibit different levels of tolerance towards isoreticular substitution. For example, while MOF-205[28] and UMCM-2[29] are both tri-module systems made from the combination between Zn_4O, a dicarboxylate, and a tricarboxylate, they are not isoreticular, suggesting the sensitivity of such platforms towards the change in ligand properties (e.g., relative size of two modules) or even the molar ratios between two modules (i.e., dicarboxylate/tricarboxylate) used in the synthesis. Therefore, to realize the potential of isoreticular chemistry under chemically challenging situations, a critical first step is to identify or create a MOF platform highly tolerant with the change in structural building blocks.

Pore space partition (PSP) proves to be a powerful concept for creating multi-modular MOF platforms of different types.[30–34] The PSP is the segregation of larger pores into smaller pockets in order to enhance the properties such as host stability and the density of guest binding sites. These advanced features can lead to increased gas uptake capacity or selective adsorption.[35–37] A great success has been realized when the PSP concept was used to create the pacs (partitioned *acs*) system.[38–41] In a prototypical pacs system, a ditopic ligand (called L1 ligand, usually dicarboxylate, diazolate, or their mixed ditopic varieties) functions as the framework-forming module to crosslink M_3(O/OH/F) trimers into MIL-88/MOF-235 topology while a 3-connected ligand (called L2 ligand, usually a tripyridyl ligand, but can also be a metal-complex) partitions the pore space through M-N coordinative bonds. On the pacs platform, the presence of charge-, geometry-, and donor-atom-complementary L1 and L2 ligands, together with the inorganic node, ensures the creation of a tri-module system with strong inter-modular structure-directing effects. The pacs is a highly tolerant platform for the replacement of modules and is an ideal system for testing and expanding the limits of the isoreticular MOF chemistry under chemically challenging conditions such as the incorporation of coordinatively competitive functional groups in the unbound form.[31]

In this work, we undertake the challenge of introducing one or two unbound -COOH groups into the pacs system. Upon the initial success with Cr-pacs system, we undertake the greater challenge of expanding -COOH functionalized pacs materials into various homo- and heterometallic trimer compositions (**Scheme 1**). Specifically, 1,2,4-benzenetricarboxylic acid (1,2,4-H_3**btc,** $C_6H_3(COOH)_3$, trimellitic acid) and 1,2,4,5-benzenetetracarboxylic acid (1,2,4,5-H_4**btec**, $C_6H_2(COOH)_4$), pyromellitic acid) are chosen as framework-forming L1 ligands while

2,4,6-tri(4-pyridyl)-1,3,5-triazine (**tpt**), 2,4,6-tris(4-pyridyl)pyridine (**tppy**), and 1,3,5-tri(4-pyridyl)benzene (**tpbz**) are used as pore-partitioning ligand. We demonstrate the feasibility for the btc ligand to form the pacs structure through the pair of para carboxylate groups at 1- and 4-positions while keeping the -COOH at the 2-position unused. We then expand our synthetic study to the btec ligand and are able to synthesize btec-pacs structures through further optimization of synthetic conditions. The use of the $Cr(acac)_3$ metal chelate as the chromium source is enlightening since stable metal chelate complexes are generally not considered a viable source for MOF crystal growth, especially for Cr^{3+} which is already severely plagued by its kinetic inertness. Unprecedentedly, we can expand -COOH functionalized pacs materials to include various metal ion compositions from homometallic Cr^{3+} and Ni^{2+} to heterometallic Co^{2+}/V^{3+}, Ni^{2+}/V^{3+}, Co^{2+}/In^{3+}, Co^{2+}/Ni^{2+}.

As a result of such diverse inorganic compositions, the framework charge could be easily tuned from anionic (for Ni^{2+}) to cationic (for Cr^{3+}) to neutral (for M^{2+}/M^{3+} ratio =2). The charge properties of new Cr-MOFs can be further modified through reversible deprotonation and re-protonation of unbound -COOH groups. It is worth noting that achieving such a broad series of isoreticular MOFs with unbound -COOH groups and many metal compositions is very difficult to do on other MOF platforms. The broad synthetic success reported here shows the feasibility of introducing coordinatively competitive unbound functional sites by employing the intrinsic structure-directing effect of the pacs platform.

Due to the wide compositional tunability of these structures, we are able to tune the material properties in many aspects such as chemical stability and functionality, gas uptake capacity and selectivity. The Cr-based structures show superior chemical stability in boiling water. Unprecedentedly, Cr-btec-tpt is stable in both strong acid (concentrated HCl, 12 M) and strong base (10 M NaOH) with a large pH range of 16.1 (from -1.1 to 15). Such large pH range of stability is unmatched by other MOFs such as other Cr-MOFs, Zr-MOFs, and ZIFs that are well known for their chemical stability.[42–45] For example, UiO-66-$(COOH)_2$ loses crystallinity completely in 1 M NaOH. Cr-btc-tpt is an ultrastable MOF with the BET surface area of 1112 m^2/g, high CO_2 uptake (100 cm^3/g), as well as high uptakes for C_2H_2 (142 cm^3/g), C_2H_4 (111 cm^3/g), C_2H_6 (110 cm^3/g), C_3H_6 (104 cm^3/g), and C_3H_8 (94.8 cm^3/g) at 298K and 1 bar. CoNi-btec-tpt shows the moderate IAST selectivity of 6 and 5.3 for C_2H_2/C_2H_4 and C_2H_2/CO_2 separations, respectively. CoV-btec-tppy and other tppy-pacs materials show promising separation properties with high benzene/cyclohexane selectivity up to about 40.

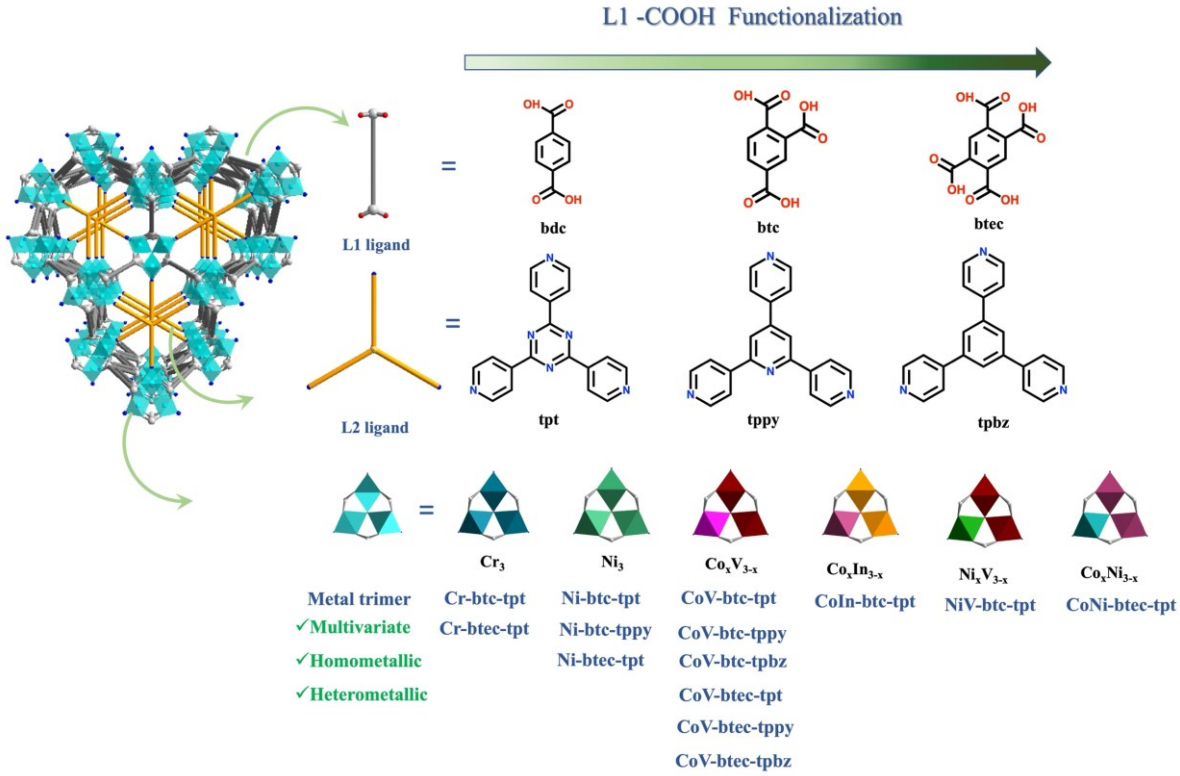

Scheme 1. Illustration of -COOH functionalized isoreticular pacs series with six types of metal trimers (M^{2+} = Co^{2+}, Ni^{2+}; M^{3+} = V^{3+}, Cr^{3+}, In^{3+}), two types of carboxyl-functionalized L1 ligands, and three types of L2 ligands. Excluding structural variations due to different ratios between two types of metal ions as well as the difference in extra-framework species, there are 36 carboxyl-functionalized pacs materials accessible from the L1/L2/M3 combinations shown above. All 6 possibilities are synthesized for the CoV composition.

2. Result and Discussion

2.1. Pushing the Limits of Isoreticular Chemistry in Ligand Functionalization and Metal Compositions

The presence of unbound functional groups in the framework is structurally and functionally interesting and significant. These functional groups can have selective interactions with guest molecules which can enable more efficient sequestration or separation.[46–49] In addition, the unbound functional groups such as carboxyl groups can offer new properties including increased proton conductivity, selective ion sensing, or acid catalytic activity.[50–52] Unbound groups such as -COOH can also be further functionalized through covalent, coordinative, or

ionic interactions. For example, H^+ of unbound -COOH can be exchanged with other cations such as different metal ions, which can be further functionalized with additional ligands.[53–55]

However, it is difficult to introduce unbound functional groups, carboxyl groups in particular, into MOFs through direct crystal growth because the strength of chemical interactions between such groups and metal ions are comparable to the interactions involved in the framework formation, and thus competing pathways exist that can disrupt isoreticular chemistry. Several methods to incorporate unbound functional groups into MOF structures have been reported so far. Among them, post-synthetic modification and direct synthesis using ligands bearing extra functional sites are the most common approaches.[56–58] Post-synthetic modifications may involve harsh reaction conditions which place some stringent requirements on chemical stability of the parent frameworks. For direct synthesis, precise tuning of synthetic conditions is often needed to control reaction pathways to achieve the desired topology while retaining free functional groups. Unfortunately, on most MOF platforms, it has been difficult to generate an isoreticular series containing substituent groups such as -COOH in unbound forms. Even if unbound -COOH can be introduced on a particular platform such as UiO-66, it is difficult to expand isoreticular MOFs by changing into different metal ions, especially those with different oxidation states and in significantly different parts of the periodic table.[59] This is because a change in metal ion type (e.g., from Cr^{3+} to Ni^{2+} to Co^{2+}/V^{3+} to Co^{2+}/In^{3+} to Ni^{2+}/V^{3+}) can dramatically alter the coordination behavior of ligands (especially for polyfunctional ligands), leading to entirely different structures (or no crystallization at all) and the failure to achieve the intended isoreticular chemistry.

In this work, by synthesizing 14 new pacs materials (**Scheme 1**), we have not only achieved the synthesis of mono- and di-carboxyl functionalized MOFs with both btc and btec ligands, but also succeeded in synthesizing these functionalized MOFs in diverse metal trimer compositions (Cr^{3+}, Ni^{2+}, Co^{2+}/V^{3+}, Ni^{2+}/V^{3+}, Co^{2+}/In^{3+}, Co^{2+}/Ni^{2+}). It is worth noting that Cr-MOFs are among the most-difficult-to-crystalize MOFs of any metal type due to the kinetic inertness of Cr^{3+}. The synthetic conditions such as acid modulators, solvent/co-solvent selections, and types of metal precursors played an important role in the synthesis of the desired phase, the degree of crystallinity, and the crystal size. For btec, more synthetic studies were performed to search for the optimum conditions.

One significant synthetic finding is that while Cr-btc-tpt was synthesized from $Cr(NO_3)_3.9H_2O$, the best result for Cr-btec-tpt was obtained by using $Cr(acac)_3$ as the Cr^{3+} precursor. Similarly, $V(acac)_3$ was used in the synthesis of NiV-btc-tpt in place of more commonly used VCl_3. Given the high stability of metal chelates due to the chelating effect,

metal chelates are not commonly used as precursors of metal ions. This work, however, shows that the use of metal chelates as precursors can be critical in the development of some highly valuable materials.

Acid modulators played a greater role in the synthesis of Cr-pacs and btec-pacs but are not essential for the synthesis of btc-pacs. Specifically, the acid modulator, acetic acid, is used in the synthesis of two Cr-MOFs. For other five btec-MOFs, different acid modulators are used (**Table S2.2**). For btc-pacs, the use of acid modulators is more for the purpose of growing large-enough crystals for single-crystal diffraction. While Cr-btc-tpt and Cr-btec-tpt were hydrothermally synthesized at 220 °C, other MOFs were synthesized solvothermally at 120 °C.

2.2. Crystal Structure Analysis of Pore-Space-Partition-Enabled Carboxyl-Functionalized Materials

Single crystal X-ray diffraction was used to determine crystal structures of Ni-btc-tpt, Ni-btc-tppy, CoIn-btc-tpt, and Ni-btec-tpt. Powder X-ray diffraction was used to confirm the phase purity by comparing the experimental PXRD patterns with the simulated patterns obtained from single crystal data of Ni-btc-tpt or Ni-btec-tpt. The framework shows the pacs-type structure with each metal atom octahedrally coordinated to the oxygen at the center of each trimer, four oxygen atoms from four different carboxylate L1 ligands, and one nitrogen atom of L2 molecule (**Figure 1**). The formular unit for the framework is $M_3(O/OH)(L1)_3(L2)$. Each unit cell contains two such formular units.

The following discussion of the crystal structural features is based on single-crystal X-ray data analysis of Ni-btc-tpt and Ni-btec-tpt. There are significant differences between btc-pacs and btec-pacs in structures and properties. For Ni-btc-tpt, the unbound carboxyl group is statistically distributed at the four sites (2,3,5,6 positions on the benzene ring) because L1 ligands are located at the 2/m symmetry site of hexagonal $P6_3/mmc$ space group.

For Ni-btec-tpt, even with a tetrafunctional L1 ligand, the framework is formed through only one pair of carboxyl groups, and the other pair at 2,5-positions remain unbound and are statistically distributed over four sites. Like Ni-btc-tpt, the unbound carboxyl groups take up the pore space adjacent to metal trimers, except that more such pore space is taken up by btec ligands due to twice as many unbound -COOH groups.

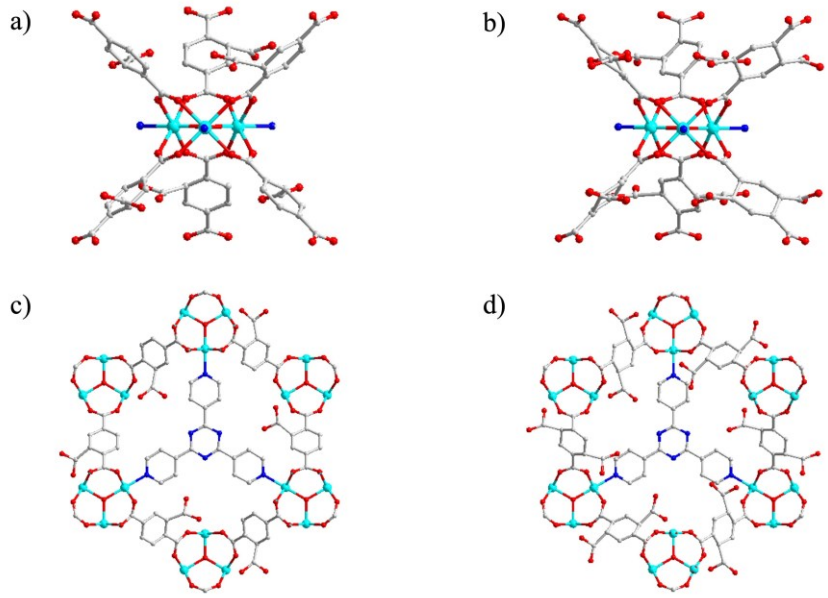

Figure 1. Crystal structures of Ni-btc-tpt and Ni-btec-tpt. a) The 9-connected trimer of Ni-btc-tpt with one unbound -COOH group. b) The 9-connected trimer of Ni-btec-tpt with two unbound -COOH groups. c) Ni-btc-tpt viewed along c-axis. d) Ni-btec-tpt viewed along c axis. Atom color code: cyan for nickel, red for oxygen, blue for nitrogen, grey for carbon.

The overall charge of the framework can be tuned with the oxidation state of metal ions within the trimer. As a result, the frameworks formed with M^{2+} metal trimers are anionic (Ni-btc-tpt, Ni-btec-tpt, Ni-btc-tppy, CoNi-btec-tpt) while the M^{3+} metal trimer gives cationic pacs (Cr-btc-tpt, Cr-btec-tpt). M^{2+}/M^{3+} combinations (CoV-btc-tpt, CoV-btec-tpt, CoV-btc-tppy, CoV-btec-tppy, CoV-btc-tpbz, CoV-btec-tpbz, CoIn-btc-tpt, NiV-btc-tpt) give neutral frameworks when the M^{2+}/M^{3+} molar ratio is 2 under the ideal situation.

In the as-synthesized forms, unbound -COOH groups remain protonated and likely hydrogen-bonded to adjacent COO^- groups that are bonded to metal trimers. As described below in the section for chemical stability, such unbound -COOH groups can be neutralized (ion-exchanged) with NaOH and re-protonated with HCl. The feasibility of tuning the framework charge using oxidation states of metal ions as well as reversible deprotonation and reprotonation of unbound -COOH groups is one of the most unique features of the pacs materials reported here.

Since each metal trimer is bonded to six COO^- groups (two COO^- links per M_3 triangular edge), significant steric repulsion between adjacent L1 ligands can be expected. The degree of the repulsion depends on the size and the number of substituents on L1. For btc-pacs, on average there are three unbound -COOH groups near the trimer whereas for btec-pacs, there are six unbound -COOH groups. We also experimented with benzenehexacarboxylic acid

($C_6(COOH)_6$, mellitic acid), but no pacs-materials were synthesized. The expected repulsion between 12 -COOH groups around the trimer should be the main reason. It is also worth noting that the pacs materials with more substituents surrounding the metal trimers, if synthesized, could be more stable from the shielding effects of the substituents.

2.3. Ultra-High Chemical Stability of Cr-based Carboxyl-Functionalized Materials.

The stability of MOFs is important for their applications. For example, the application of proton conductivity could benefit from stability in water and acidic conditions. The 14 pacs materials reported here are all stable towards activation to generate porosity for gas sorption applications (**Table S3.1**), however, their chemical stability in water (also boiling water) or under different pH values vary significantly depending on specific M3-L1-L2 compositions. Compared to prototypical benzenedicarboxylate (**bdc**) based pacs materials, btc-pacs and btec-pacs materials can be more susceptible to the attack by polar solvents due to the presence of extra polar groups (-COOH) on L1 ligands. For example, Ni_3-btc-tpt and Ni_3-btec-tpt pacs are not stable in water as evidenced by their loss of crystallinity after soaking in water (**Figure S2.2**). Fortunately, the chemical stability can be tuned with metal trimers. The highest stability in the carboxyl-functionalized pacs family was found in Cr-btc-tpt and Cr-btec-tpt. In the octahedral configuration, Cr(III)-MOFs offer the advantage of high ligand-field stabilization energy due to its d^3 electronic configuration. From the perspective of hard-soft acid-base principle, hard-acid Cr^{3+} has a strong bonding interaction with hard carboxylate groups, adding to the strength of the Cr-carboxylate linkage.[60]

The stability of Cr-btc-tpt and Cr-btec-tpt pacs was studied by refluxing in boiling water and soaking in concentrated acid (12M HCl) and basic solutions (1M to 10M NaOH) for 24 or 48 hours. The PXRD patterns of the materials treated under the above conditions were compared with the pristine pacs. The PXRD patterns indicate that both Cr-btc-tpt and Cr-btec-tpt retained their high crystallinity in boiling water and concentrated HCl (**Figures 2a and 2b**). The nitrogen gas sorption at 77K (**Figures 2c and 2d**) indicates that both Cr-btc-tpt and Cr-btec-tpt retained their N_2 uptakes after treatments with either the boiling water or concentrated HCl. In-fact, Cr-btec-tpt shows higher N_2 uptake after treatment probably due to better activation from treatments with boiling water and strong acid.

The stability under basic conditions is also interesting and impressive. It is more complicated due to the presence of unbound -COOH groups and different number of them in btc and btec materials. The PXRD shows that both Cr-btc-tpt and Cr-btec-tpt are stable when

treated in 1M to 5M NaOH solutions (**Figures 2a and 2b**). Cr-btec-tpt showed better stability in more basic solutions than Cr-btc-tpt based on the observation that Cr-btec-tpt could withstand 10 M NaOH for 48 hours whereas Cr-btc-tpt starts to collapse in 10M NaOH solution after 24 hours and decomposes completely after 48 hours of soaking.

The study by nitrogen adsorption at 77K shows a decrease in gas uptakes after the NaOH treatments (Figures 2c and 2d). It is worth noting that the decrease in N_2 uptake is unlikely due to the loss of crystallinity from the framework collapse. The replacement of H^+ in unbound COOH by sodium ion plays a key role. This is due to the neutralization reaction between the dangling -COOH and NaOH solution, leading to the formation of the -COONa salt. The higher base stability of Cr-btec-tpt compared to Cr-btc-tpt may be related to the greater amount of Na^+ inclusion in Cr-btec-tpt, because twice as many Na^+ ions can be included into Cr-btec-tpt than in Cr-btc-tpt. The presence of Na^+ ions adjacent to -COO groups may provide greater steric hindrance to better shield the metal trimers from attack by OH^-, thus making Cr-btec-tpt more stable than Cr-btc-tpt under highly basic conditions.

The presence of sodium ion was supported by Energy Dispersive X-ray Spectroscopy (EDS) analysis of the samples after the NaOH treatment. The measured Na/Cr ratio ranges from 0.82 to 1.2 for Cr-btc-tpt and 1.8 to 2.4 for Cr-btec-tpt. Given the framework formula of $(Cr_3O)(L1)_3(L2)$, the above measured Na/Cr ratios are consistent with the theoretical numbers of unbound -COOH groups per Cr atom in the framework (1 in btc-pacs and 2 in btec-pacs), indicating that unbound -COOH groups were nearly stoichiometrically ion-exchanged (neutralized) with NaOH to form -COONa. The incorporation of Na^+ ions in the framework thus reduces nitrogen uptakes due to the increased molecular weight and the possible pore blockage from the Na^+ ion (and its hydration sphere if not thoroughly activated).

The reversibility of deprotonation and re-protonation of the unbound -COOH groups and their effects on N_2 adsorption were tested by soaking Cr-btec-tpt in 1M, 5M, and 10 M NaOH solutions for 48h followed by soaking in 12 M HCl for 24h (**Figures 2d**). While the N_2 uptake first decreases on NaOH treatments, these samples regain their initial N_2 uptakes upon subsequent HCl treatment. Such reversible N_2 uptakes after sequential base-acid treatments further confirm the ultra-high stability of Cr-btec-tpt. Furthermore, these results also show that the -COOH groups are initially present in the protonated form in the pristine pacs and can be reversibly deprotonated and re-protonated by increasing or decreasing the pH of the solution, respectively. The ultrahigh stability and the acidic nature of Cr-btec-tpt suggest its potential use as a solid weak-acid catalyst.

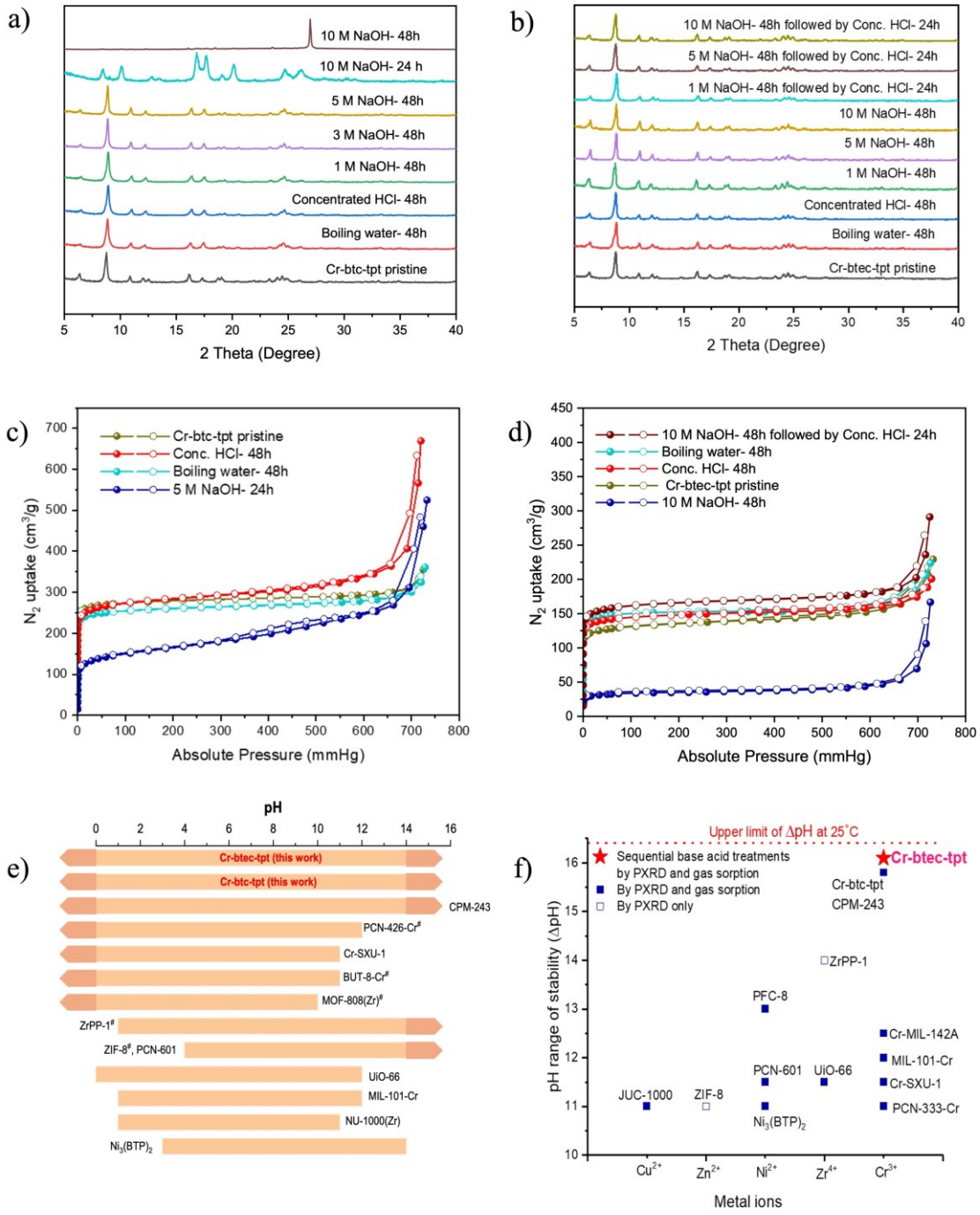

Figure 2. Chemical stability of Cr-btc-tpt and Cr-btec-tpt under harsh conditions. PXRD of Cr-btc-tpt (a) and Cr-btec-tpt (b) after boiling water, acid and base treatments; N_2 isotherms of Cr-btc-tpt (c) and Cr-btec-tpt (d); (e) Comparison of stability with other MOFs. The arrow indicates stability at pH< 0 or pH> 14. # indicates stability determined from PXRD; (f) The stability range defined by the difference between the lowest and the highest pH values for select MOFs. The red dotted line is the maximum limit of the pH range (16.4) from 12 M HCl (pH = -1.1) to 19M NaOH (pH = 15.3).

To compare the stability of Cr-btec-tpt with non-carboxyl-functionalized material, CPM-243(ac) (Cr-bdc-tpt-ac, made with CH_3COOH modulator) was first treated with 10 M NaOH for 48 hours and followed by 12 M HCl. The NaOH-treated CPM-243(ac), upon further HCl treatment, instantly gets digested giving a clear solution (**Figure S2.7**). This implies that Cr-btec-tpt is more stable than CPM-243(ac). **Figures 2e and 2f** compare the chemical stability of Cr-btec-tpt with other highly respected stable MOFs.[42,43,45,60–65] It is remarkable that Cr-btec-tpt is not only stable over the widest pH range (from -1.1 to 15), but it also retains its robustness after cycle of extreme pH treatments.

2.4. Gas Sorption Properties

Nitrogen adsorption-desorption isotherms at 77K confirmed the permanent porosity of all 14 pacs materials synthesized in this work (**Figure S3.1**). For 8 btc-pacs, the Brunauer–Emmett–Teller (BET) surface area ranges from 591.4 m^2/g for Ni-btc-tppy to 1112 m^2/g for Cr-btc-tpt (**Table 1**). The btec-pacs materials have lower surface area than btc-pacs (from 278.0 m^2/g for CoNi-btec-tpt to 592.3 m^2/g for Cr-btec-tpt) likely due to the presence of the extra -COOH group. Cr-pacs materials have the highest surface area in either the btc family or the btec family. While there are MOFs with much higher surface areas than the Cr-pacs materials reported here, their chemical stabilities (and uptake capacities for CO_2 and hydrocarbon gases under ambient conditions) are often much lower than Cr-pacs materials.

Table 1. Gas sorption and separation properties of btc and btec pacs materials.

Name	BET surface area (m^2/g)	Uptake at 1 bar and 298K (cm^3/g)						IAST Selectivity for 50/50 mixtures			
		CO_2	C_2H_2	C_2H_4	C_2H_6	C_3H_6	C_3H_8	C_2H_2/CO_2	C_2H_2/C_2H_4	C_2H_6/C_2H_4	C_3H_6/C_3H_8
Cr-btc-tpt	**1112**	**100.2**	**142.1**	**110.5**	**109.8**	104.1	94.8	4.2	2.3	1.3	1.4
Ni-btc-tpt	865.5	81.6	118.0	85.7	83.2	88.4	79.5	4.4	2.0	1.2	1.5
Ni-btc-tppy	591.4	58.4	88.2	65.7	64.9	78.7	70.0	4.5	2.6	-	-
CoV-btc-tpt	752.3	82.1	113.9	92.0	89.2	96.4	88.3	3.6	2.0	1.2	1.4
CoV-btc-tppy	783.2	82.4	112.9	88.6	88.6	97.7	88.1	3.7	2.1	1.2	1.5
CoV-btc-tpbz	805.5	78.1	113.9	85.7	85.1	95.2	84.9	3.7	2.0	1.3	1.5
CoIn-btc-tpt	866.6	92.1	123.9	100.8	102.0	**110.1**	**101.7**	2.9	1.6	1.3	1.3
NiV-btc-tpt	798.5	-	-	-	-	-	-	-	-	-	-
Cr-btec-tpt	592.3	59.6	68.2	55.9	54.0	55.4	49.8	3.6	1.7	1.3	1.4
Ni-btec-tpt	351.2	47.9	62.4	39.6	37.2	50.3	43.4	3.9	3.5	-	1.9
CoV-btec-tpt	455.5	48.1	63.6	49.8	49.7	57.2	52.7	**5.5**	2.9	-	1.7
CoV-btec-tppy	469.5	42.5	56.5	37.5	36.8	48.7	43.0	4.4	3.9	-	1.9
CoV-btec-tpbz	551.9	48.1	56.7	35.4	34.4	52.8	43.8	4.3	4.3	-	1.8
CoNi-btec-tpt	278.0	37.9	52.3	31.2	26.9	44.3	40.0	5.3	**6.0**	1.4[a)]	1.4

a) (Shows C_2H_4/C_2H_6 selectivity)

These pacs materials has two cage types: a triagonal-bipyramidal cage (t2-cage) made of five trimers and an octahedral cage (o-cage) made of six trimers (**Figure S1.17**). The diameters of the t2 cage calculated from the crystal structures for Ni-btc-tpt and Ni-btec-tpt are 6.69 Å and 6.63 Å, respectively. The diameters of the o-cage were calculated to be 4.95 Å and 5.07 Å for Ni-btc-tpt and Ni-btec-tpt, respectively. These cage diameters are larger than the kinetic diameters of small hydrocarbon molecules such as CO_2, C_2H_2, C_2H_4, C_2H_6, C_3H_6 and C_3H_8 (**Table S5.3**). To evaluate applications of these new pacs materials for gas storage and separation, adsorption-desorption isotherms of CO_2, C_2H_2, C_2H_4, C_2H_6, C_3H_6 and C_3H_8 gases were systematically studied at 298K and 273K (**Figures S4**). The uptake capacities of these pacs materials are particularly impressive and are in fact outstanding compared to other highly stable MOFs or carboxyl-functionalized MOFs. Similar to the trend in the surface area, for all gases, btc-pacs materials have higher uptake capacity than corresponding btec-pacs materials.

For CO_2, these pacs materials show high uptakes such as 100.2 and 59.6 cm^3/g for Cr-btc-tpt and Cr-btec-tpt, 81.6 and 47.9 cm^3/g for Ni-btc-tpt and Ni-btec-tpt, 82.1 and 48.1 cm^3/g for CoV-btc-tpt and CoV-btec-tpt (1 bar and 298K). These values (especially 100.2 cm^3/g for Cr-btc-tpt) compare favorably with some other stable MOFs such as JUC-1000 (80 cm^3/g at 298K), [66] UiO-66 (64.5 cm^3/g at 273K),[67] NU-1000 (39.2 cm^3/g at 293K),[68] and solvent-free-synthesized CPM-243 (90 cm^3/g at 298K).[31] The high uptake, combined with high chemical stability, enables Cr-pacs materials for potential applications involving CO_2 capture or reduction under harsh conditions.

The C_2H_2 uptakes at 298K are considerably higher and the adsorption isotherms much steeper compared to CO_2, C_2H_4, and C_2H_6 gases (**Figures S4.1-S4.24**). The C_2H_2 uptakes of select pacs materials at 1 bar and 298K are 142.1 vs. 68.2 cm^3/g for Cr-btc-tpt vs. Cr-btec-tpt, 118.0 vs. 62.4 cm^3/g for Ni-btc-tpt vs. Ni-btec-tpt, and 113.9 vs. 63.6 cm^3/g for CoV-btc-tpt vs. CoV-btec-tpt. Noticeably, Cr-btc-tpt (142.1 cm^3/g at 298K) outperforms most top-preforming MOF adsorbents such as UTSA-222a (103.4 cm^3/g),[69] UTSA-300 (69 cm^3/g),[70] JNU-1(63 cm^3/g),[71] and SNNU-98-Co (72 cm^3/g).[72] Another interesting aspect is that both btc and btec pacs materials show high C_2H_2 uptakes at low pressure region (<0.1 bar). C_2H_2 uptakes of the btc pacs (Cr-btc-tpt, Ni-btc-tpt) at 0.1 bar and 298K are 59.5 cm^3/g and 40.3 cm^3/g (**Figure 4a**), whereas the btec pacs materials (Cr-btec-tpt, Ni-btec-tpt) show uptakes of 33.5 cm^3/g and 29.9 cm^3/g at 0.1 bar and 298K (**Figure 4b**). **Table S5.1** compares the acetylene uptakes of the btc and btec pacs at around 0.1 bar with some of the best performing MOFs.

The C_2H_4 uptakes for select pacs materials reported here are 110.5 vs. 55.9 cm^3/g for Cr-btc-tpt vs. Cr-btec-tpt, 85.7 vs. 39.6 cm^3/g for Ni-btc-tpt vs. Ni-btec-tpt, and 92.0 vs. 49.8 cm^3/g for CoV-btc-tpt vs. CoV-btec-tpt at 1 bar and 298K. Interestingly, the C_2H_6 uptakes are very similar to C_2H_4 uptakes, as shown by C_2H_6 uptakes of 109.8 vs. 54.0 cm^3/g for Cr-btc-tpt vs. Cr-btec-tpt, 83.2 vs. 37.2 cm^3/g for Ni-btc-tpt vs. Ni-btec-tpt, and 89.2 vs. 49.7 cm^3/g for CoV-btc-tpt vs. CoV-btec-tpt. Apart from CoNi-btec-tpt (IAST selectivity 1.4 for C_2H_4/C_2H_6), all other pacs materials reported here are ethane-selective with IAST selectivity (C_2H_6/C_2H_4) around 1.3. It is worth noting that the IAST selectivity for inverse C_2H_6-selective C_2H_6/C_2H_4 separation is typically below 2 and the higher inverse selectivity is usually accompanied by much lower uptake capacity (sometimes much lower sample stability as well). In the pacs materials reported here, the C_2H_6 uptake capacity of Cr-btc-tpt (109.8 cm^3/g) is higher than most of the ethane-selective MOFs such as PCN-245 (73.2 cm^3/g, C_2H_6/C_2H_4 selectivity = 1.8),[73] ZIF-8 (45.4 cm^3/g, C_2H_6/C_2H_4 selectivity = 1.8),[74,75] and ZIF-7 (41.1 cm^3/g, C_2H_6/C_2H_4 selectivity = 1.5).[76] The overall separation performance of the pacs materials can be boosted by their significantly higher-than-normal uptake capacities for C_2H_4 and C_2H_6.

The C_3H_6 uptakes for select pacs materials at 298K and 1 bar are 104.1 and 55.4 cm^3/g for Cr-btc-tpt and Cr-btec-tpt. For all btc and btec pacs materials, C_3H_8 uptakes are slightly lower than C_3H_6 values and are 94.8 and 49.8 cm^3/g for Cr-btc-tpt and Cr-btec-tpt. The C_3H_6 uptakes of these pacs are higher than some top performing MOFs such as Co-gallate (40.3 cm^3/g),[77] KAUST-7 (44.8 cm^3/g),[78] Y-abtc (44.8 cm^3/g).[79] A steep rise in C_3H_6 and C_3H_8 adsorption isotherms and high uptake at low pressure region (<0.1 bar) are seen in both btc and btec pacs. At around 0.1 bar pressure and 298K, Cr-pacs materials show the C_3H_6 uptake of 82.4 cm^3/g and 43.9 cm^3/g for Cr-btc-tpt and Cr-btec-tpt, respectively (**Figure S9.3**). The IAST selectivity of these pacs materials for C_3H_6/C_3H_8 are generally around 1.5-1.9. Combined with high uptake values, such selectivity is capable of the C_3H_6/C_3H_8 separation.

To evaluate the effect of L2 ligand on properties of btc and btec pacs, L2 ligand was tuned from tpt to tppy and tpbz in CoV-btc and CoV-btec pacs. Overall, it can be said that tpt, tppy, and tpbz offer comparable high gas sorption performance for the CoV compositions studied here. However, the benzene/cyclohexane selectivity can be much improved by optimizing the L2 ligand as described in Section 2.6.

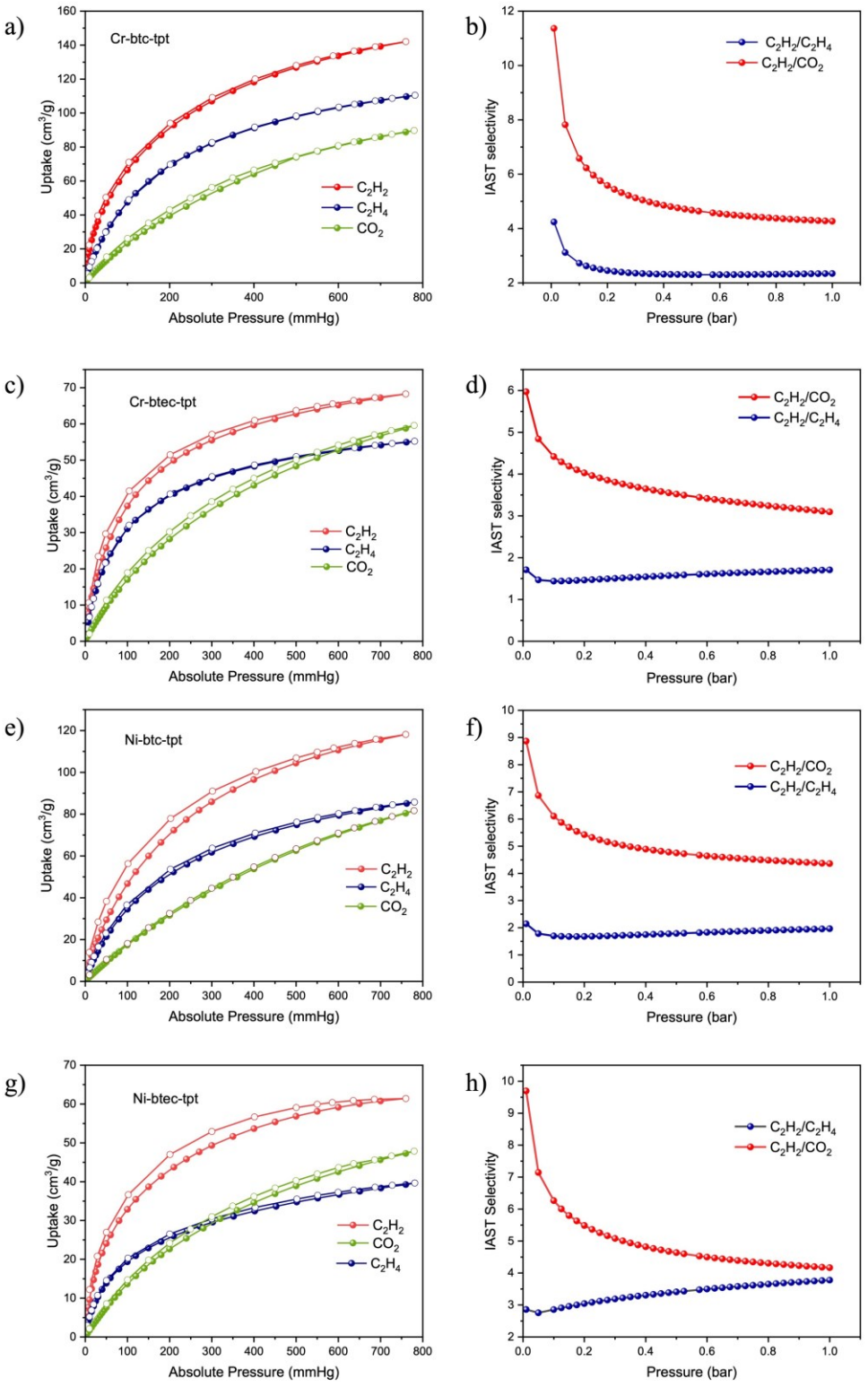

Figure 3. C_2H_2, C_2H_4 and CO_2 isotherms of Cr-btc-tpt (a), Cr-btec-tpt (c), Ni-btc-tpt (e), and Ni-btec-tpt (g) at 298K. The IAST selectivity for C_2H_2/CO_2 and C_2H_2/C_2H_4 at 298K for Cr-btc-tpt pacs (b), Cr-btec-tpt (d), Ni-btc-tpt (f), and Ni-btec-tpt (h).

For the btc composition, the BET surface areas are 752.3, 783.2, and 805.5 m^2/g for CoV-btc-tpt, CoV-btc-tppy, and CoV-btc-tpbz, respectively. In the same L2 sequence and at 1 bar and 298K, the CO_2 uptakes are 82.1, 82.4, and 74.1 cm^3/g, the C_2H_2 uptakes are 113.8, 112.9, and 113.8 cm^3/g, and the C_2H_4 uptakes are 92.0, 88.7, 85.7cm^3/g. It is clear that in addition to tpt, other L2 ligands can also offer high adsorption performance.

For the btec composition, the BET surface areas are 455.5, 469.5, 551.9 m^2/g for CoV-btec-tpt, CoV-btec-tppy, and CoV-btec-tpbz, respectively. In the same L2 sequence and at 1 bar and 298K, the CO_2 uptakes are 48.1, 42.5, and 40.7 cm^3/g, the C_2H_2 uptakes are 63.6, 56.5, and 56.7 cm^3/g, and the C_2H_4 uptakes are 49.8, 37.5, and 35.4 cm^3/g. Overall, the uptakes of these pacs materials decrease slightly from tpt to tppy to tpbz. Corresponding, the IAST selectivity for C_2H_2/C_2H_4 separation increases from 2.9 to 3.9 to 4.3, but the C_2H_2/CO_2 selectivity shows a slight decrease from 5.5 to 4.4 to 4.3 from tpt to tppy to tpbz (**Table S3.2**)

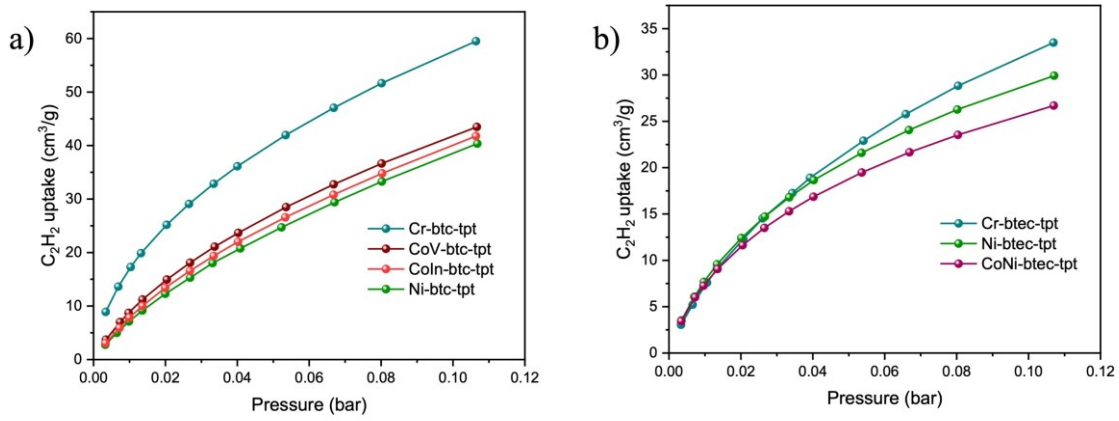

Figure 4. C_2H_2 uptakes of a) btc and b) btec pacs at low pressure region at 298K.

To evaluate the potential of these new pacs materials for industrial gas separation, the IAST selectivity for C_2H_2/C_2H_4 and C_2H_2/CO_2 separations were calculated. **Table S3.2** shows the IAST selectivity of btc and btec pacs. The IAST selectivity of Ni-btec-tpt is 3.5 for C_2H_2/C_2H_4 and 3.9 for C_2H_2/CO_2. Its uptake capacity at 1 bar and 298K is 62.4 cm^3/g for C_2H_2, 47.9 cm^3/g for CO_2, and 39.6 cm^3/g for C_2H_4. Three cycles of column breakthrough experiments were carried out on Ni-btec-tpt pacs to evaluate the actual separation efficiency. From the experimental breakthrough curves (**Figures 5a and 5b**), the breakthrough time for C_2H_2/CO_2 separation is around 40 minutes while for C_2H_2/C_2H_4 separation, the breakthrough time is around 20 minutes. Based on the results from multiple breakthrough cycles, Ni-btec-tpt is stable towards gas separation and can achieve the selective separation of C_2H_2/C_2H_4 and C_2H_2/CO_2 mixtures.

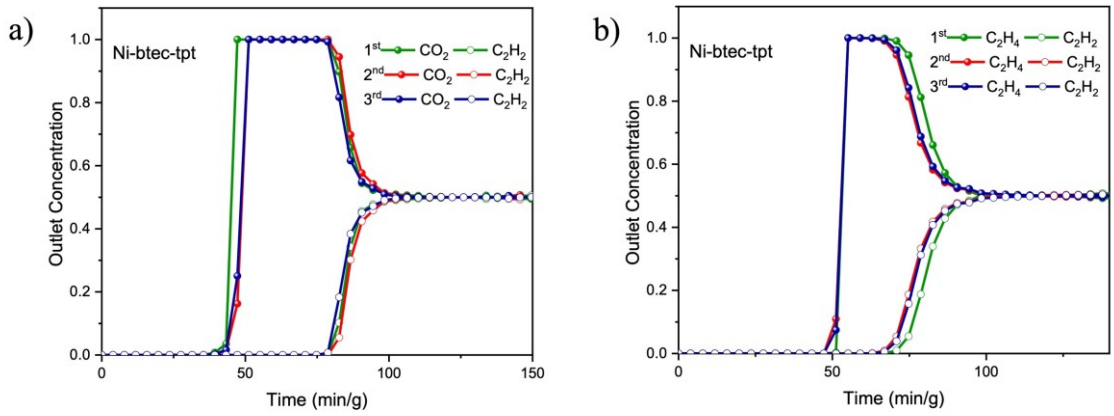

Figure 5. Three cycles of breakthrough curves of Ni-btec-tpt at 1 atm and 298K for a) C_2H_2/ CO_2 separation with a flow of C_2H_2/ CO_2 /He (1/1/2 mL/min). b) C_2H_2/C_2H_4 separation with a flow of C_2H_2/ C_2H_4 /He (1/1/2 mL/min).

2.6. Benzene/Cyclohexane Separation Properties.

Cyclohexane is an important petrochemical used in the production of various intermediates. However, its production results in a mixture of benzene and cyclohexane that must be separated to produce pure cyclohexane. Benzene-selective adsorptive removal of benzene from C_6H_6/C_6H_{12} over porous materials can directly yield pure cyclohexane. Vapor sorption experiments from a mixture of benzene and cyclohexane were carried out on Ni-btc-tpt, Ni-btc-tppy and Ni-btec-tpt and the separation efficiency was studied using nuclear magnetic resonance spectroscopy (^{1}H NMR). ^{1}H NMR spectra of the Ni-pacs materials after the sorption experiments are given in the supporting information. Ni-btc-tpt has benzene/cyclohexane selectivity of about 14 whereas Ni-btec-tpt shows a selectivity of about 17 (**Table S4.1**). The selectivity can be further improved by tuning L2 ligand. Changing the L2 ligand from tpt in Ni-btc-tpt to tppy in Ni-btc-tppy enhances the selective interaction with benzene molecules, leading to a higher selectivity of about 38 for benzene/cyclohexane mixtures compared to Ni-btc-tpt pacs (14). A higher preference for benzene can be seen and the affinity for benzene over cyclohexane increases with the number of carboxyl groups. This shows the preferential interaction of the aromatic hydrogens with the framework oxygen atoms. In addition, the planar benzene molecule might be more permeable to the confined pores than the twisted cyclohexane molecule. Based on these results, these Ni-based frameworks show capability to separate C_6H_6/C_6H_{12} mixtures.

3. Conclusion

We have demonstrated the feasibility of introducing competing unbound functional groups into MOF structures by employing the inter-modular structure directing effects of the pacs platform. The synthesis of an isoreticular series of the pore-space-partitioned frameworks based on btc and btec ligands opens up new possibilities among the pore-partitioned materials. These novel frameworks offer great potentials in the separation and purification applications of small hydrocarbon molecules. Importantly, the Cr-based frameworks (Cr-btc-tpt and Cr-btec-tpt) provide two novel chemically stable MOFs with high porosity and potential for post-synthetic modifications. The properties of these frameworks can be further enhanced, and new potential applications can be discovered through post-synthetic modifications of the unbound -COOH to generate new functional sites.

[CCDC 2239850, 2246486, 2266503 and 2266527 contains the supplementary crystallographic data for this paper. These data can be obtained free of charge from The Cambridge Crystallographic Data Centre via www.ccdc.cam.ac.uk/data_request/cif.]

Supporting Information

Supporting Information is available from the Wiley Online Library or from the author.

Acknowledgements

We acknowledge the support of this work by the US Department of Energy, Office of Basic Energy Sciences, Materials Sciences and Engineering Division under Award No. DE-SC0010596 (P.F.). Single-crystal X-ray diffraction studies were performed on an instrument purchased with an NSF MRI grant (CHEM 2117040, X.B.).

Received: ((will be filled in by the editorial staff))

Revised: ((will be filled in by the editorial staff))

Published online: ((will be filled in by the editorial staff))

References

[1] H. Jiang, D. Alezi, M. Eddaoudi, *Nat Rev Mater* **2021**, *6*, 466.
[2] Z. Mai, D. Liu, *Cryst Growth Des* **2019**, *19*, 7439.
[3] Z. Chen, S. L. Hanna, L. R. Redfern, D. Alezi, T. Islamoglu, O. K. Farha, *Coord Chem Rev* **2019**, *386*, 32.
[4] *J Am Chem Soc* **2016**, *138*, 15507.
[5] M. Eddaoudi, J. Kim, N. Rosi, D. Vodak, J. Wachter, M. O'Keeffe, O. M. Yaghi, *Science (1979)* **2002**, *295*, 469.
[6] J. Liu, B. Lukose, O. Shekhah, H. K. Arslan, P. Weidler, H. Gliemann, S. Bräse, S. Grosjean, A. Godt, X. Feng, K. Müllen, I.-B. Magdau, T. Heine, C. Wöll, *Sci Rep* **2012**, *2*, 921.
[7] S. R. Caskey, A. G. Wong-Foy, A. J. Matzger, *J Am Chem Soc* **2008**, *130*, 10870.
[8] L. J. Wang, H. Deng, H. Furukawa, F. Gándara, K. E. Cordova, D. Peri, O. M. Yaghi, *Inorg Chem* **2014**, *53*, 5881.
[9] W. Fan, X. Zhang, Z. Kang, X. Liu, D. Sun, *Coord Chem Rev* **2021**, *443*, 213968.
[10] N. M. Padial, C. Chinchilla-Garzón, N. Almora-Barrios, J. Castells-Gil, J. González-Platas, S. Tatay, C. Martí-Gastaldo, *J Am Chem Soc* **2023**, *145*, 21397.
[11] X. Wang, H. Liu, M. Sun, H. Wang, X. Feng, W. Chen, X. Feng, W. Fan, D. Sun, *ACS Appl Mater Interfaces* **2024**, *16*, 7819.
[12] A. Dutta, Y. Pan, J.-Q. Liu, A. Kumar, *Coord Chem Rev* **2021**, *445*, 214074.
[13] P. Deria, J. E. Mondloch, O. Karagiaridi, W. Bury, J. T. Hupp, O. K. Farha, *Chem Soc Rev* **2014**, *43*, 5896.
[14] O. Karagiaridi, W. Bury, A. A. Sarjeant, C. L. Stern, O. K. Farha, J. T. Hupp, *Chem Sci* **2012**, *3*, 3256.
[15] Q. Yang, S. Vaesen, F. Ragon, A. D. Wiersum, D. Wu, A. Lago, T. Devic, C. Martineau, F. Taulelle, P. L. Llewellyn, H. Jobic, C. Zhong, C. Serre, G. De Weireld, G. Maurin, *Angewandte Chemie International Edition* **2013**, *52*, 10316.
[16] D.-Q. Chu, C.-L. Pan, L.-M. Wang, J.-Q. Xu, *Mendeleev Communications* **2002**, *12*, 207.
[17] C. Volkringer, T. Loiseau, N. Guillou, G. Férey, M. Haouas, F. Taulelle, E. Elkaim, N. Stock, *Inorg Chem* **2010**, *49*, 9852.
[18] X.-C. Huang, Y.-Y. Lin, J.-P. Zhang, X.-M. Chen, *Angewandte Chemie International Edition* **2006**, *45*, 1557.
[19] S. S.-Y. Chui, S. M.-F. Lo, J. P. H. Charmant, A. G. Orpen, I. D. Williams, *Science (1979)* **1999**, *283*, 1148.
[20] S. Surblé, C. Serre, C. Mellot-Draznieks, F. Millange, G. Férey, *Chemical Communications* **2006**, 284.
[21] G. Férey, C. Serre, C. Mellot-Draznieks, F. Millange, S. Surblé, J. Dutour, I. Margiolaki, *Angewandte Chemie International Edition* **2004**, *43*, 6296.
[22] Y. Liu, J. F. Eubank, A. J. Cairns, J. Eckert, V. Ch. Kravtsov, R. Luebke, M. Eddaoudi, *Angewandte Chemie International Edition* **2007**, *46*, 3278.
[23] H. Li, M. Eddaoudi, M. O'Keeffe, O. M. Yaghi, *Nature* **1999**, *402*, 276.
[24] J. H. Cavka, S. Jakobsen, U. Olsbye, N. Guillou, C. Lamberti, S. Bordiga, K. P. Lillerud, *J Am Chem Soc* **2008**, *130*, 13850.
[25] Y. Liu, J. F. Eubank, A. J. Cairns, J. Eckert, V. Ch. Kravtsov, R. Luebke, M. Eddaoudi, *Angewandte Chemie International Edition* **2007**, *46*, 3278.
[26] F. Millange, C. Serre, G. Férey, *Chemical Communications* **2002**, 822.
[27] A. Cadiau, J. S. Lee, D. Damasceno Borges, P. Fabry, T. Devic, M. T. Wharmby, C. Martineau, D. Foucher, F. Taulelle, C.-H. Jun, Y. K. Hwang, N. Stock, M. F. De

Lange, F. Kapteijn, J. Gascon, G. Maurin, J.-S. Chang, C. Serre, *Advanced Materials* **2015**, *27*, 4775.
[28] J. Sim, H. Yim, N. Ko, S. B. Choi, Y. Oh, H. J. Park, S. Park, J. Kim, *Dalton Transactions* **2014**, *43*, 18017.
[29] K. Koh, A. G. Wong-Foy, A. J. Matzger, *J Am Chem Soc* **2009**, *131*, 4184.
[30] X. Zhao, X. Bu, Q.-G. Zhai, H. Tran, P. Feng, *J Am Chem Soc* **2015**, *137*, 1396.
[31] Y. Xiao, Y. Chen, A. N. Hong, X. Bu, P. Feng, *Angewandte Chemie International Edition* **2023**, *62*, e202300721.
[32] Y. Chen, H. Yang, W. Wang, X. Li, Y. Wang, A. N. Hong, X. Bu, P. Feng, *Small* **2023**, *19*, 2303540.
[33] A. N. Hong, E. Kusumoputro, Y. Wang, H. Yang, Y. Chen, X. Bu, P. Feng, *Angewandte Chemie International Edition* **2022**, *61*, e202116064.
[34] W. Wang, Y. Chen, P. Feng, X. Bu, *Advanced Materials* **2024**, *n/a*, 2403834.
[35] Q.-G. Zhai, X. Bu, X. Zhao, D.-S. Li, P. Feng, *Acc Chem Res* **2017**, *50*, 407.
[36] Q.-G. Zhai, X. Bu, C. Mao, X. Zhao, L. Daemen, Y. Cheng, A. J. Ramirez-Cuesta, P. Feng, *Nat Commun* **2016**, *7*, 13645.
[37] X. Zhao, X. Bu, Q.-G. Zhai, H. Tran, P. Feng, *J Am Chem Soc* **2015**, *137*, 1396.
[38] H. Yang, Y. Chen, C. Dang, A. N. Hong, P. Feng, X. Bu, *J Am Chem Soc* **2022**, *144*, 20221.
[39] Y. Wang, X. Jia, H. Yang, Y. Wang, X. Chen, A. N. Hong, J. Li, X. Bu, P. Feng, *Angewandte Chemie International Edition* **2020**, *59*, 19027.
[40] A. N. Hong, H. Yang, T. Li, Y. Wang, Y. Wang, X. Jia, A. Zhou, E. Kusumoputro, J. Li, X. Bu, P. Feng, *ACS Appl Mater Interfaces* **2021**, *13*, 52160.
[41] Y. Wang, X. Zhao, H. Yang, X. Bu, Y. Wang, X. Jia, J. Li, P. Feng, *Angewandte Chemie International Edition* **2019**, *58*, 6316.
[42] K. S. Park, Z. Ni, A. P. Côté, J. Y. Choi, R. Huang, F. J. Uribe-Romo, H. K. Chae, M. O'Keeffe, O. M. Yaghi, *Proceedings of the National Academy of Sciences* **2006**, *103*, 10186.
[43] K. Leus, T. Bogaerts, J. De Decker, H. Depauw, K. Hendrickx, H. Vrielinck, V. Van Speybroeck, P. Van Der Voort, *Microporous and Mesoporous Materials* **2016**, *226*, 110.
[44] E.-X. Chen, M. Qiu, Y.-F. Zhang, Y.-S. Zhu, L.-Y. Liu, Y.-Y. Sun, X. Bu, J. Zhang, Q. Lin, *Advanced Materials* **2018**, *30*, 1704388.
[45] H. He, Q. Sun, W. Gao, J. A. Perman, F. Sun, G. Zhu, B. Aguila, K. Forrest, B. Space, S. Ma, *Angewandte Chemie International Edition* **2018**, *57*, 4657.
[46] Z. Xiang, S. Leng, D. Cao, *The Journal of Physical Chemistry C* **2012**, *116*, 10573.
[47] R. Colorado-Peralta, J. María Rivera-Villanueva, J. Manuel Mora-Hernández, D. Morales-Morales, L. Ángel Alfonso-Herrera, *Polyhedron* **2022**, *224*, 115995.
[48] Z. H. Rada, H. R. Abid, H. Sun, J. Shang, J. Li, Y. He, S. Liu, S. Wang, *Progress in Natural Science: Materials International* **2018**, *28*, 160.
[49] X. Wang, M. Xu, W. Fan, D. Sun, *Chin J Chem* **2023**, *41*, 3772.
[50] Z. Sun, S. Yu, L. Zhao, J. Wang, Z. Li, G. Li, *Chemistry – A European Journal* **2018**, *24*, 10829.
[51] W. Sun, J. Wang, G. Zhang, Z. Liu, *RSC Adv* **2014**, *4*, 55252.
[52] Y. Zhang, C. Huang, L. Mi, *Dalton Transactions* **2020**, *49*, 14723.
[53] L. Zhang, L. Li, E. Hu, L. Yang, K. Shao, L. Yao, K. Jiang, Y. Cui, Y. Yang, B. Li, B. Chen, G. Qian, *Advanced Science* **2020**, *7*, 1901918.
[54] F. Ragon, B. Campo, Q. Yang, C. Martineau, A. D. Wiersum, A. Lago, V. Guillerm, C. Hemsley, J. F. Eubank, M. Vishnuvarthan, F. Taulelle, P. Horcajada, A. Vimont, P. L. Llewellyn, M. Daturi, S. Devautour-Vinot, G. Maurin, C. Serre, T. Devic, G. Clet, *J Mater Chem A Mater* **2015**, *3*, 3294.

[55] X. Wang, H. Liu, Y. Li, X. Yang, F. Gao, X. Wang, Z. Kang, W. Fan, D. Sun, *Coord Chem Rev* **2023**, *482*, 215093.
[56] S. J. Garibay, Z. Wang, K. K. Tanabe, S. M. Cohen, *Inorg Chem* **2009**, *48*, 7341.
[57] S. J. Garibay, S. M. Cohen, *Chemical Communications* **2010**, *46*, 7700.
[58] F. Zhou, J. Zhou, X. Gao, C. Kong, L. Chen, *RSC Adv* **2017**, *7*, 3713.
[59] Q. Yang, S. Vaesen, F. Ragon, A. D. Wiersum, D. Wu, A. Lago, T. Devic, C. Martineau, F. Taulelle, P. L. Llewellyn, H. Jobic, C. Zhong, C. Serre, G. De Weireld, G. Maurin, *Angewandte Chemie International Edition* **2013**, *52*, 10316.
[60] H. Yang, F. Peng, A. N. Hong, Y. Wang, X. Bu, P. Feng, *J Am Chem Soc* **2021**, *143*, 14470.
[61] X. Lian, D. Feng, Y.-P. Chen, T.-F. Liu, X. Wang, H.-C. Zhou, *Chem Sci* **2015**, *6*, 7044.
[62] K. Wang, X.-L. Lv, D. Feng, J. Li, S. Chen, J. Sun, L. Song, Y. Xie, J.-R. Li, H.-C. Zhou, *J Am Chem Soc* **2016**, *138*, 914.
[63] V. Colombo, S. Galli, H. J. Choi, G. D. Han, A. Maspero, G. Palmisano, N. Masciocchi, J. R. Long, *Chem Sci* **2011**, *2*, 1311.
[64] E.-X. Chen, M. Qiu, Y.-F. Zhang, Y.-S. Zhu, L.-Y. Liu, Y.-Y. Sun, X. Bu, J. Zhang, Q. Lin, *Advanced Materials* **2018**, *30*, 1704388.
[65] J.-H. Wang, Y. Zhang, M. Li, S. Yan, D. Li, X.-M. Zhang, *Angewandte Chemie International Edition* **2017**, *56*, 6478.
[66] H. He, Q. Sun, W. Gao, J. A. Perman, F. Sun, G. Zhu, B. Aguila, K. Forrest, B. Space, S. Ma, *Angewandte Chemie International Edition* **2018**, *57*, 4657.
[67] S. Biswas, P. Van Der Voort, *Eur J Inorg Chem* **2013**, *2013*, 2154.
[68] P. Deria, J. E. Mondloch, E. Tylianakis, P. Ghosh, W. Bury, R. Q. Snurr, J. T. Hupp, O. K. Farha, *J Am Chem Soc* **2013**, *135*, 16801.
[69] J. Ma, J. Guo, H. Wang, B. Li, T. Yang, B. Chen, *Inorg Chem* **2017**, *56*, 7145.
[70] R.-B. Lin, L. Li, H. Wu, H. Arman, B. Li, R.-G. Lin, W. Zhou, B. Chen, *J Am Chem Soc* **2017**, *139*, 8022.
[71] H. Zeng, M. Xie, Y.-L. Huang, Y. Zhao, X.-J. Xie, J.-P. Bai, M.-Y. Wan, R. Krishna, W. Lu, D. Li, *Angewandte Chemie International Edition* **2019**, *58*, 8515.
[72] J.-W. Wang, S.-C. Fan, H.-P. Li, X. Bu, Y.-Y. Xue, Q.-G. Zhai, *Angewandte Chemie International Edition* **2023**, *62*, e202217839.
[73] D. Lv, R. Shi, Y. Chen, Y. Wu, H. Wu, H. Xi, Q. Xia, Z. Li, *ACS Appl Mater Interfaces* **2018**, *10*, 8366.
[74] U. Böhme, B. Barth, C. Paula, A. Kuhnt, W. Schwieger, A. Mundstock, J. Caro, M. Hartmann, *Langmuir* **2013**, *29*, 8592.
[75] O. T. Qazvini, R. Babarao, Z.-L. Shi, Y.-B. Zhang, S. G. Telfer, *J Am Chem Soc* **2019**, *141*, 5014.
[76] C. Gücüyener, J. van den Bergh, J. Gascon, F. Kapteijn, *J Am Chem Soc* **2010**, *132*, 17704.
[77] B. Liang, X. Zhang, Y. Xie, R.-B. Lin, R. Krishna, H. Cui, Z. Li, Y. Shi, H. Wu, W. Zhou, B. Chen, *J Am Chem Soc* **2020**, *142*, 17795.
[78] A. Cadiau, K. Adil, P. M. Bhatt, Y. Belmabkhout, M. Eddaoudi, *Science (1979)* **2016**, *353*, 137.
[79] H. Wang, X. Dong, V. Colombo, Q. Wang, Y. Liu, W. Liu, X.-L. Wang, X.-Y. Huang, D. M. Proserpio, A. Sironi, Y. Han, J. Li, *Advanced Materials* **2018**, *30*, 1805088.